

Testing and finite element modeling of stressed skin diaphragms

Yang Liu[†] and Qilin Zhang[‡]

Department of Building Engineering, Tongji University, Shanghai 200092, China

Weijun Qian^{‡†}

Zhejiang Jingong Steel Building Construction Group Co., Ltd., Shaoxing 312030, China

(Received November 15, 2005, Accepted October 13, 2006)

Abstract. The cold formed light-gauge profiled steel sheeting can offer considerable shear resistance acting in the steel building frame. This paper conducted the full-scale test on the shear behavior of stressed skin diaphragm using profiled sheeting connected by the self-tapping screws. A three-dimensional finite element model that simulates the stressed skin diaphragm was developed. The sheet was modeled using thin element model while the supporting members were simulated using beam elements. Fasteners were represented in the numerical model as equivalent springs. A joint test program was conducted to characterize the properties of these springs and results were reported in this study. Finite element model of the full-scale test was analyzed by use of the ANSYS package, considering nonlinearity caused by the large deflection and slip of fasteners. The experimental data was compared with the results acquired by the EUR formulas and finite element analysis.

Keywords: shear diaphragm; profiled sheeting; testing; finite element analysis.

1. Introduction

The use of profiled sheeting in the construction of building structures offers many advantages as it leads to structures that are lightweight, cost effective and durable. If proper connections are made between the profiled steel sheeting and structure members, the cold formed light-gauge profiled steel panels can offer considerable shear resistance acting in the steel building frame, which not only increase the whole rigidity of structure, but also as an important part of main body. This kind of advantageous behavior of profile sheeting is usually named the stressed skin diaphragm.

Early work on corrugated metal sheeting acting as diaphragm was carried out by Nilson (1968) and provided the basis for the American Iron and Steel and Institute Manual on the Design of Light Gauge Steel Diaphragms (AISI 1967). The production of the British manual for the design of stressed skin structures (1972) was based upon the work of El-Dakhkhni (1976) and Bryan (1968). This work was

[†]Ph.D., Corresponding author, E-mail: liuyanghit@tom.com

[‡]Professor

^{†‡}Engineer

improved and extended by Davies (1976, 1977) and Easley (1977). Fazio *et al.* (1978) extended Easley's theory and development simple formulas to predict shear capacity of diaphragms with any type of fasteners, whether weld, rivets, or screws.

Finite element analysis of the metal deck shear diaphragms was carried out by Nilson and Ammar (1974). El-Dakhkhni (1976) described a method for calculating the shear flexibility of light gauge partitions using a strain energy approach taking into consideration the different modes of attachments. Significant contributions to the knowledge of shear diaphragm have been made by Easley (1975), Luttrell (1971), Davies and Fisher (1979) and Easterling and Porter (1994).

Due to its complex assembly of light gauge steel sections and fasteners, the mathematical analysis of these shear diaphragms are complex. Presently, there are mainly three kinds of methods to determine the shear strength and stiffness of diaphragm panels, including tests and numerical simulation and simple analytical procedures.

This paper conducted full-scale diaphragm tests on the shear behavior of stressed skin diaphragm using profiled sheets connected by the self-tapping screws, which is constructed according to the detailing in engineering practice in china. Because the diaphragms are tested full size, this makes experimental work very expensive and time consuming. Furthermore, tests give only limited information as it is generally only possible to measure loads and deflections. With increases in the power of computers and rapid development in computer software, numerical simulation has become a very powerful tool in mechanical engineering. Numerical simulation provides a relatively inexpensive, and time efficient alternative to physical experiments.

The objective of numerical investigation presented in this paper is to develop an advanced non-linear finite element model (FEM) on the shear behavior of stressed skin diaphragm. Finite element program ANSYS (2004) was used to perform the numerical analysis. The results of finite element analysis (FEA) were compared with those obtained from the full-scale test and those calculated by the EUR formulation.

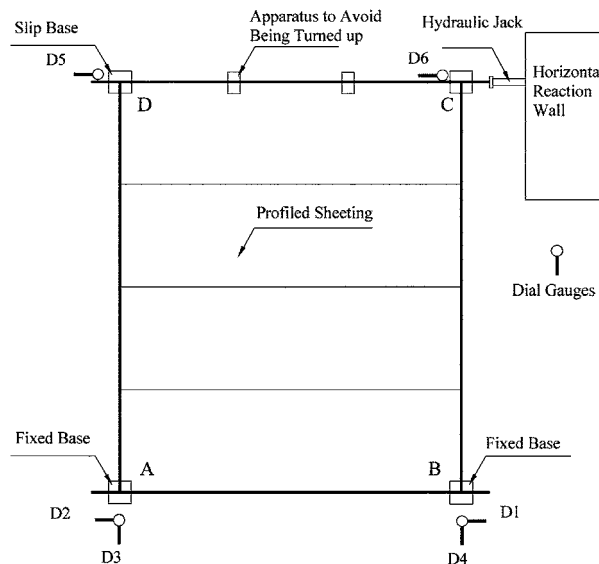


Fig. 1 Plan of cantilever beam diaphragm test

2. Full scale tests

Test diaphragms consisted of profiled sheeting, frame members and fasteners. Tests of cantilever horizontal diaphragm were used here, with the load applied parallel to the direction of span of the sheeting as shown in Fig. 1.

Profiled sheeting named HV-225 and HV-248 were 3.2 m long, which widely used in the building system in china. The cross sections of the profiled sheeting are shown in Fig. 2. All the profiled sheeting had a thickness of 0.6 mm.

Four full width profiled sheeting were fastened together to constitute the full-scale test specimen. A plan view of the tested diaphragm is shown in Fig. 3. Member arrangement for cantilever diaphragm is

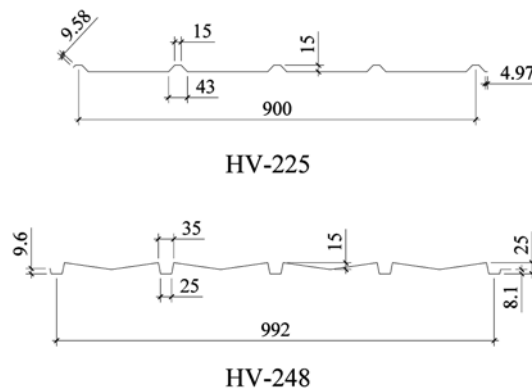


Fig. 2 Cross sections of the profiled sheeting

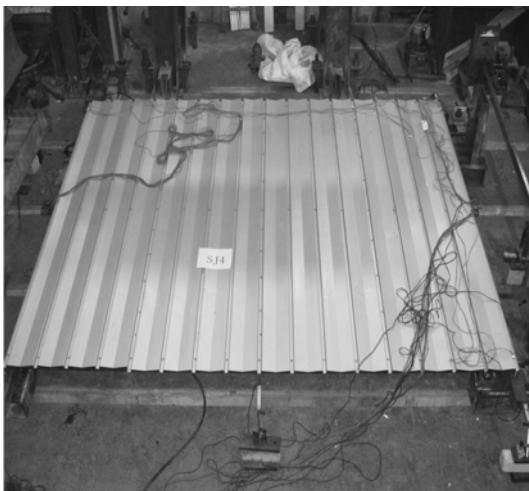


Fig. 3 Plan view of the tested diaphragm

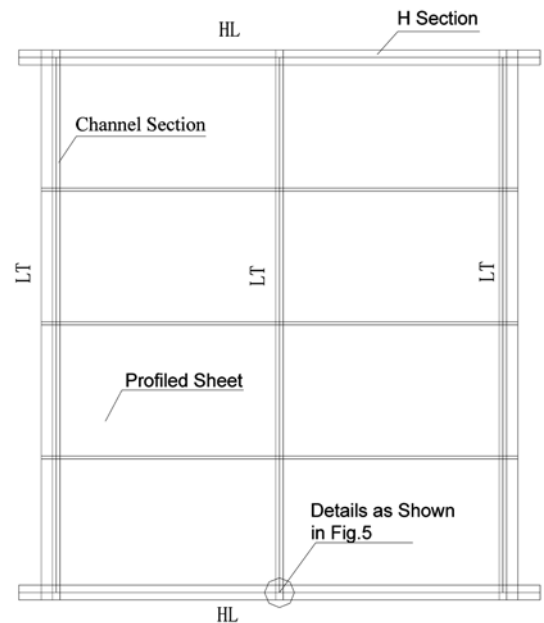


Fig. 4 Member arrangement for cantilever diaphragm

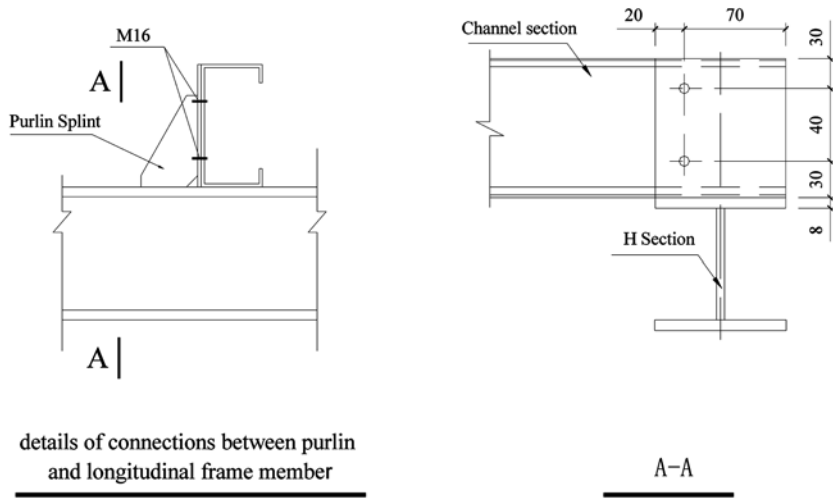


Fig. 5 Details of connections between the purlin and longitudinal frame member

shown in Fig. 4. The profiled sheeting were supported on a number of purlins aligned in the direction perpendicular to the sheeting. The purlins, which were made of cold-formed beam, were supported on longitudinal frame members. the details of the connection are shown in Fig. 5. The purlins are *Channel* section designated as C100×50×20×2.5(100×50×20×2.5 mm). Longitudinal frame members are *H* section, designated as H100×100×8×6(100×100×8×6 mm). The flange of purlin was connected to the sheets using the self-tapping screws in every trough of the corrugated sheeting. The fastener locations are shown in Fig. 6.

According to the sectional configuration of sheet and arrangement of connections, the experimental program consisted of four test series labeled as T1, T2, T3 and T4. Two identical specimens are for the test series T1 and T3. Series of diaphragm specimens are shown in Table 1.

Four dial gauges were attached to the fixed bases to measure the body rotation of the test rig during the test. In addition, the deflection at the end of longitudinal frame member was measured. The locations of these points are shown in Fig. 1.

Load was applied to the sheeting through the longitudinal frame members which are themselves eccentricities to the sheeting. As such in the third and two part of the longitudinal frame member

Table 1 Series of diaphragm specimens

Test Series number	Specimens number	Fasteners space (mm)		Purlin space d_3 (mm)	Specimen dimensions $B \times L$ (mm)	Sectional configuration of sheeting
		Between sheeting and purlin d_1	Between the sheeting d_2			
T1	SJ1-1	225	1500	1500	3600*3000	HV-225
	SJ1-2	225	1500	1500	3600*3000	HV-225
T2	SJ2	225	1000	1000	3600*3000	HV-225
T3	SJ3-1	248	1500	1500	4000*3000	HV-248
	SJ3-2	248	1500	1500	4000*3000	HV-248
T4	SJ-4	248	1500	250	4000*3000	HV-248

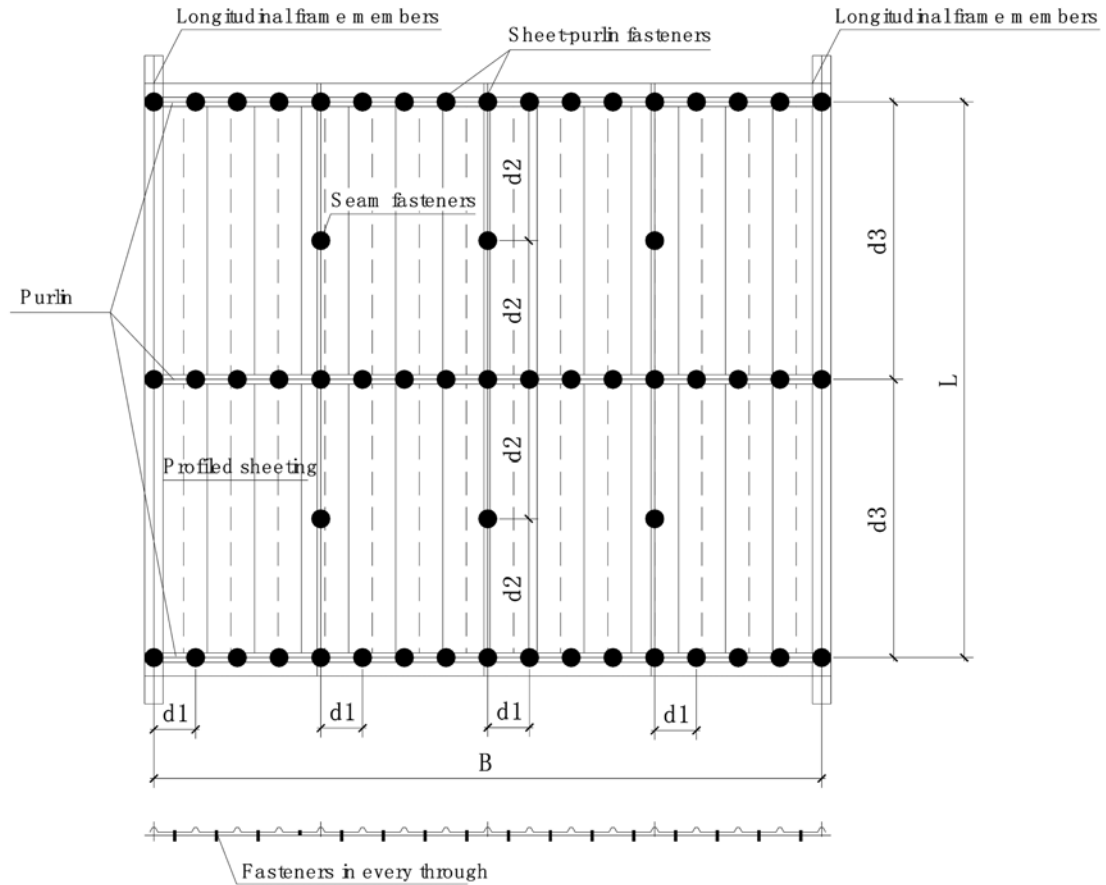
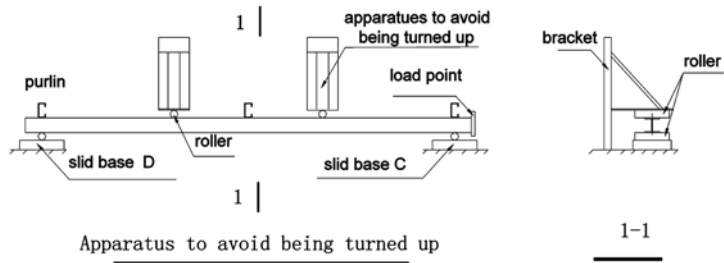


Fig. 6 Definitions of the fastener locations

position the trolleys were used to prevent the panel from being turned up as shown in Fig. 7.

Prior to the proffed sheeting being fixed, preliminary tests were conducted. The shear loads were small and it was difficult to load the test frame by the hydraulic jack. As such two representative specimens (SJ1-1 and SJ3-1) were tested as shown in the Fig. 8. Typical load displacement curves for the preliminary tests are shown in Fig. 9. From the slope of the load-displacement curves, it is shown that the test frames had negligible stiffness.

The load was applied to the end of frame member in the form of shear load. The location of this specific point 'C' is shown in Fig. 1. A 50KN hydraulic jack was applied the loads in plane of the panels. Test procedure was to the first load the diaphragm in three increments up to 20 percentage of the ultimate load estimated, maintaining this load for ten minutes in order to observe whether any creep occurred. The diaphragm was then unloaded and the percentage recovery noted. The diaphragm was then loaded to failure in the several staged, and the load was increased gradually. After each increment, the deflections were again measured and an examination made for signs of damage or distress. As the failure load was approached the load increments were maintained for fifteen minutes before the deflections were measured.



Tester photo

Fig. 7 Apparatus to avoid being turned up

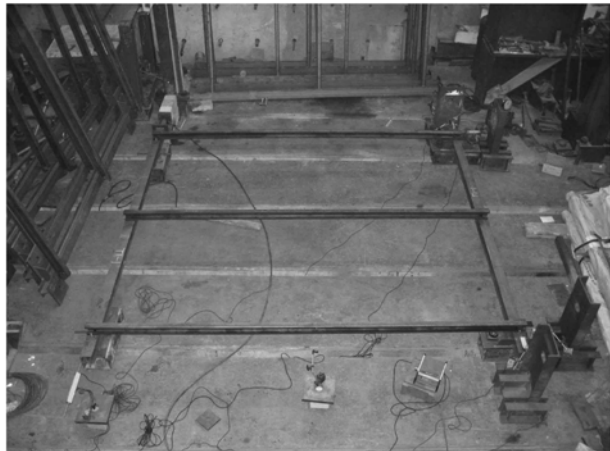


Fig. 8 Preliminary frame test in progress

3. Fastener shear tests

The fasteners are those connecting the sheeting to the supporting structure (sheet to purlin) which may be named ‘thin to thick’ fasteners because they connect the relatively thin sheeting to the thicker members below and those connecting side laps between adjacent sheets (seam fasteners) which may be

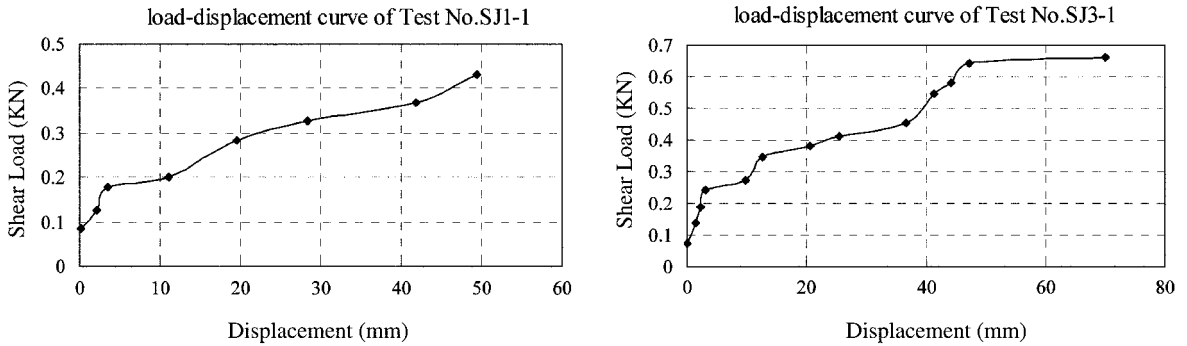
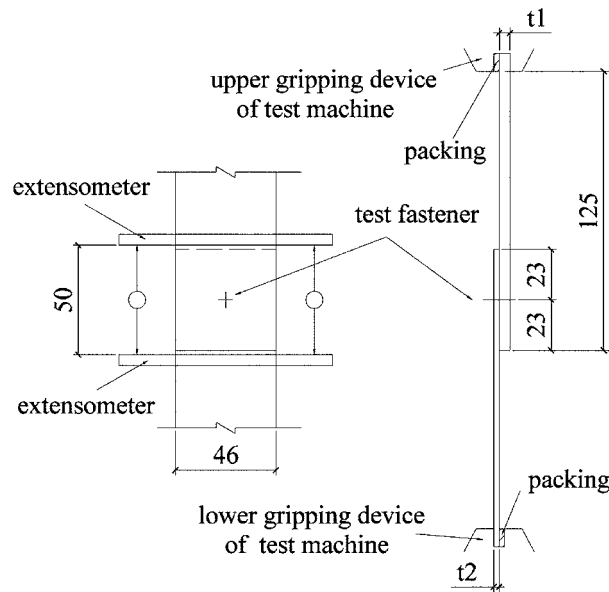


Fig. 9 Load-displacement curves of preliminary frame test



Unit: mm

Fig. 10 Schematic diagram test set-up

termed 'thin to thin' fasteners.

The fasteners were simulated as a continuous spring system in the finite element model having two horizontal component that simulates the stiffness provided by the fastener in the in-plane transverse direction of the panel, and vertical component that simulates the stiffness provided by the fastener in the in-plane axis direction of the panel. Joint tests program were conducted in this section in order to characterize these spring systems.

The specimen test was known as the 'single lap joint shear test' in which a fasteners lap joint of standard dimensions was placed in a tensile testing machine and loaded to failure. Two series specimens were conducted in this paper. Five identical specimens of each series were tested in order to quantify the behavior of the fasteners connecting side laps between adjacent sheeting. A schematic diagram of the test set-up and test in progress are shown in Fig. 10 and Fig. 11.



(a) Self-tapping screws; straps 0.6/0.6 mm



(b) Self-tapping screws; straps 0.6/2.5 mm

Fig. 11 Shear test in progress

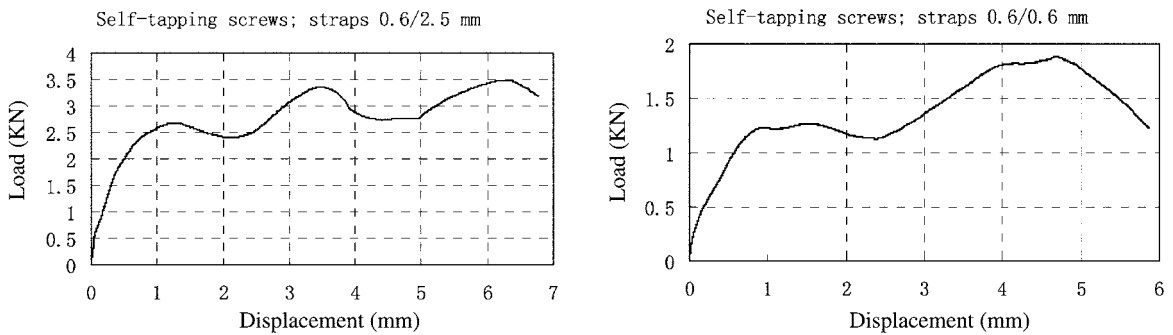


Fig. 12 Typical load-displacement curves

The tests were conducted and tested in a load-controlled manner with an incremental rate of 1KN/min (initial stages of testing), and in a displacement-controlled manner with rate of 1 mm/min (later stages of testing). During the test, load-displacement readings should be recorded every 1 second. The five specimens of two series failed at average loads equal to 1.27 KN and 2.4 KN, respectively. Failure was defined as the maximum load recorded during the test or load at which the first significant drop occurs in the load-displacement diagram. A typical load displacement curves for the tested specimens are shown in Fig. 12.

4. Finite element analysis

4.1 General

Finite element program ANSYS Version 9.0 [2004] is used to simulate the shear behavior of stressed skin diaphragm. The measure cross-section dimensions and spring properties of the test specimens are included in the finite element model.

Non-linear analysis is performed using the Newton-Raphson procedure. The total load is applied in a sequence of incremental load steps. Within each step, the nonlinear equilibrium equations are linearized through a tangent stiffness approach. Iterations at constant external load are performed to remove residual (unbalanced) forces arising from the use of linearized equilibrium equations. At the end of each step, total equilibrium conditions are satisfied within a small prescribed tolerance.

4.2 Type of element and finite element mesh

The stressed diaphragms are simulated in the model using finite elements such as beam, shell and spring element. The profile sheeting is modeled using three dimensional thin shell elements with four nodes and six degrees of freedom per node, which are translations in the x , y , z global directions and rotations about the x , y and z global directions. The thin shell elements have both membrane and bending capabilities: Purlin, which eventually support the sheeting through fasteners, are modeled using beam elements, as well as longitudinal frame members. Frame elements had six degrees of freedom per node.

A complication arises at the intersection between the two sheeting at the seam location, at the intersection between the sheeting and purlin, as well as at the intersection between the sheeting and frame members. Detailed finite element modeling of intersection is very difficult to achieve. As such it is decided to simulate the fasteners connecting sheet and frame members as a system of continuous springs with three components: two horizontal components that simulate the stiffness provided by the fastener in the in-plane transverse direction of the panel, and vertical component that simulates the stiffness provided by the fastener in the in-plane axis direction of the panel.

When the behavior associated with a certain degree of freedom is assessed, the other two degrees of freedom are kept restrained. It is anticipated that in the advanced non-linear range of behavior some degree of coupling exists between the three degrees of freedom. It is well known that the axis stiffness is more quantitative than the transverse stiffness and is assumed to be infinite here. A representation of these springs is provided in Fig. 13.

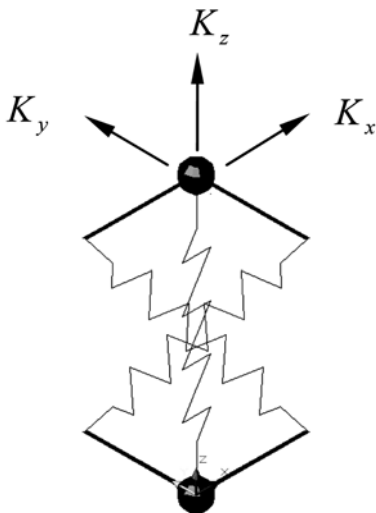


Fig. 13 Finite element simulation of fastener

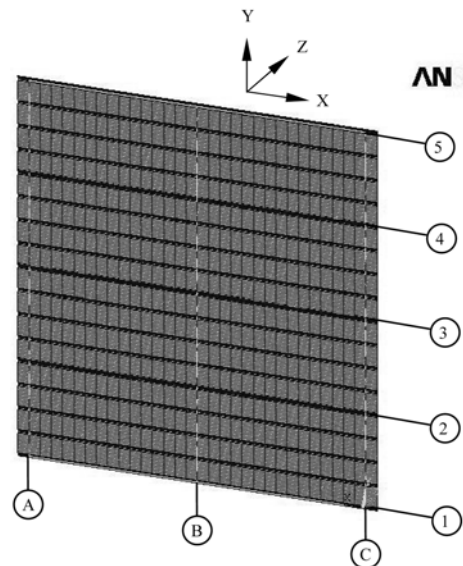


Fig. 14 Finite element mesh

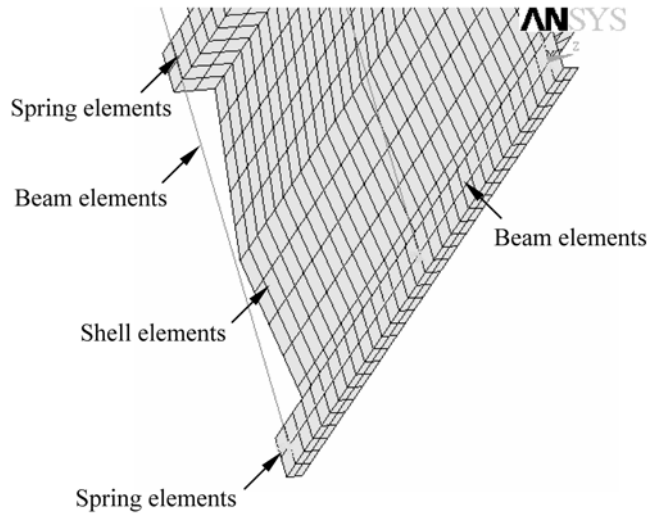


Fig. 15 Details of the finite element mesh

A finite element mesh developed to simulate one of the full-scale tests described in the previous section is shown in Fig. 14. Having discretised the purlin, frame member and the sheeting the connected point can be thought of as nodes with dependent degrees of freedom and related by the spring elements.

Axes A, B and C and axes 1 and 5 represent purlin and longitudinal frame members. At the intersection of these axes, a double node concept is applied and the displacement along the X, Y and Z axes were coupled together. At intersection of axes A, B and C and axes 1, 2, 3, 4 and 5: at these locations, sheeting is connected to the purlin and longitudinal frame members by self-tapping screws that are modeled as a spring system. The self-tapping screws in every or alternate though of the profiled sheeting are also modeled as a spring system. Details of the finite elements mesh are shown in Fig. 15.

4.3 Equivalent horizontal spring properties of fasteners and material properties

The fasteners are modeled using a nonlinear spring system with spring constants, which permit connection of and movement between sheeting and the frame members at the fastener locations. The force-displacement characteristics for the spring elements are determined, based on the result of joint

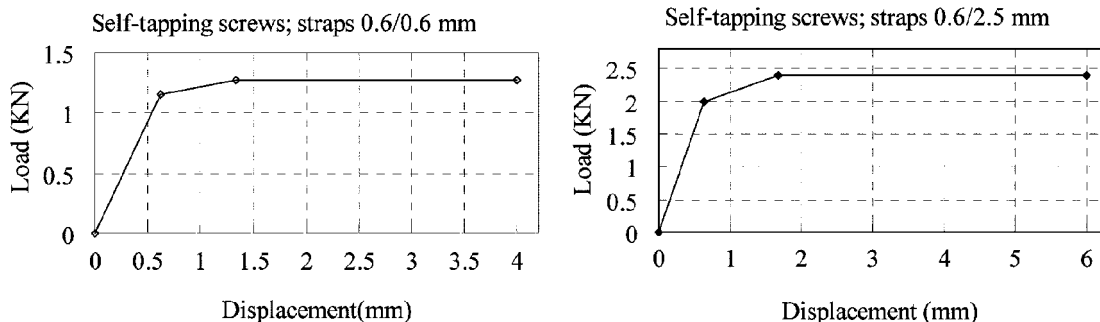


Fig. 16 Force-displacement fitted curves for the spring element

Table 2 Material properties of the steel-as used in the FEA

Thickness (mm)	Yield strength f_y (Mpa)	Ultimate tensile strength f_u (Mpa)	Yield Ratio f_y / f_u	Elongation f (%)
2.5	356.5	503	0.71	32.6
0.6	410	445	0.92	29

tests described in the previous section. For nonlinear analysis, three line segments along fitted curves are used to the force-displacement and instantaneous stiffness characteristics, as is shown in Fig. 16. These values are incorporated into a three-dimensional finite element model consisting of a combination of shell and frame elements.

The steel material is isotropic with an elastic modulus E of 206000 Mpa and Poisson's ratio of 0.3. The properties of the steel were also measured using the standard tensile test. The average measured values are given in Table 2.

4.4 Boundary condition and loading method

The fixed-ended boundary condition is simulated by restraining all the degrees of freedom of the nodes at both ends of one frame member, except for the translational degree of freedom in the axial direction. Apparatus to avoid being turned up is simulated by restraining the degrees of freedom of the node of the longitudinal frame member along the z direction.

The displacement control loading method, which is identical to that used in the experimental program, is used in the finite element analysis. Displacement was applied to the nodes at end of the longitudinal frame member along the X direction, see Fig. 14.

5. EUR formulas for shear strength and stiffness of the stressed skin diaphragms

In order to give comparisons with the results of the tests and FEA, the design method of European Recommendations for the Application of Metal Sheeting acting as a Diaphragm (EUR 1995) is proposed and the design formulation is presented according to the format of EUR.

5.1 Shear strength

The shear strength of the stressed skin diaphragms should normally by considering failure modes in the end shear panels and by the failure of connections between sheeting and frame members. The ultimate strength V_{ult} associated with these failure modes may be obtained as follows:

5.1.1 Seam capacity

Strength due to seam fasteners:

$$V_{ult} = n_s F_s + \frac{\beta_1}{\beta_2} n_p F_p \quad (1)$$

where n_s is the number of seam fastener per side lap, F_s is the design strength of an individual seam

fastener, n_p is the number of purlins, F_p is the design strength of an individual sheet/purlin fastener, β_1 is a factor to allow for the number of sheet/purlin fasteners per sheet width, $\beta_2 = (n_f - 1) / n_f$ for sheeting, $\beta_3 = 1.0$ for decking and n_f is the number of sheet/purlin fasteners per sheet width.

5.1.2 Shear connector fastener capacity

Strength due to sheet-beam or sheet-column fasteners:

$$V_{ult} = n_{sc} F_{sc} \quad (\text{at end gables}) \quad (2)$$

where n_{sc} is the number of sheet/shear connector fasteners per end rafter and F_{sc} is the design strength of an individuals sheet/shear connector fastener.

$$V_{ult} = n'_{sc} F_{sc} \quad (\text{at internal rafters}) \quad (3)$$

Where P_{ult} is the ultimate load at a shear panel point, n'_{sc} is the number of sheet/shear connector fasteners per internal rafter and n is the number of shear panels in the length of the diaphragm assembly.

5.1.3 Two sides of shear panels fastened

For sheeting attached to the purlins only and to the end rafters:

(1) capacity of end fasteners in an internal shear panel

$$P_{ult} = \beta_2 n_p F_p \quad (4)$$

(2) capacity of purlin /rafter connections

$$P_{ult} = n_p F_{pr} \quad (5)$$

Where F_{pr} is the design strength of a purlin/rafter connection and β_2 is a factor to allow for the number of sheet/purlin fasteners per sheet width.

5.1.4 Shear bulking

Shear stresses may cause (1) local buckling of wide flanges and webs of the trapezoidal sheeting and (2) global bucking of the diaphragm as a whole.

For global shear buckling:

$$V_g = \frac{14.4}{b} D_x^{1/4} D_y^{3/4} (n_p - 1)^2 \quad (6)$$

Where D_x and D_y are the orthogonal bending stiffnesses given by:

$$D_x = \frac{Et^3 d}{12(1 - \nu^2)u}$$

$$D_y = \frac{EI}{d}$$

Where E is the modulus of elasticity of steel, t is the net sheet thickness, d is the pitch of the

corrugations, ν is Poisson's ratio for steel and u is the perimeter length of a complete single corrugation of pitch d .

For local buckling:

$$V_g = \frac{36b}{b_k^2} D_x^{1/4} D_y^{3/4} \quad (7)$$

5.1.5 No permissible modes

In order to prevent collapse or gross distortion of the profile at the end of the sheeting, the following limitation on shear force in a shear panel should be observed:

Every corrugation fastened at the end of the sheeting:

$$0.9t^{1.5}bf_y/d^{0.5} \geq V^* \quad (8)$$

Alternate corrugation fastened at the end of the sheeting:

$$0.3t^{1.5}bf_y/d^{0.5} \geq V^* \quad (9)$$

Where t is the net sheet thickness, b is the depth of a shear panel in a direction parallel to the corrugations, f_y is the design yield stress of steel and d is the pitch of the corrugations

5.1.6 Design shear capacity

The design shear capacity V^* may be taken as the least of the values of V_{ult} given 5.1.1 and 5.1.2, and the derived values of V_{ult} , given by $V_{ult} = \frac{1}{2}P_{ult}(n-1)$ in 5.1.3, as appropriate to the case considered. It should be checked that the capacity in the other failure modes is greater than V^* as given 5.1.5 and 5.1.6.

5.2 Shear flexibility and stiffness

Shear flexibility is that the displacement per unit shear load. The total shear flexibility of a shear panel is the summation of components of the various factors involved. The main components considered are due to: shear deformation of sheets (c_1), bending or distortion of corrugation profile (c_2), axial deformation of the frame (c_3) and fastener deformation (c_4, c_5).

Therefore, $c_s = c_1 + c_2 + c_3 + c_4 + c_5 = 1/k_s$.

5.2.1 Flexibility due to shear deformation of sheet (c_1)

Applying strain energy approach the flexibility may be derived as:

$$c_1 = \frac{2a(1+\nu)[1+(2h/d)]}{Et b} \quad (10)$$

Where a is the width of a shear panel in a direction perpendicular to the corrugations, ν is Poisson's ratio, h is the height of the sheeting profile and d is the pitch of the corrugations.

5.2.2 Flexibility due to bending of corrugation profile (c_2)

This flexibility will be dependant on the manner of attachment of the sheeting to the surround frame. The flexibility due to bending or distortion of corrugation profile, c_2 , can be expressed as:

$$c_2 = \frac{ad^{2.5} \alpha_1 \alpha_2 K}{Et^{2.5} b^2} \quad (11)$$

Where α_1, α_2 are factors to allow for intermediate purlins and number of sheet lengths, K is a sheeting constant which can obtain from Davies and Bryan (1982) or EUR (1995).

5.2.3 Flexibility due to fastener deformation (c_{31}, c_{32}, c_{33})

The shear transfer between the sheet and frame members at the fastener points causes a stress concentration which results in deformation of light gauge material. This contributes to the sheet flexibility.

For sheet to purlin fastener, the flexibility can be expressed as:

$$c_{31} = \frac{2as_p p}{b^2} \quad (12)$$

Where s_p is the slip per seam fastener per unit load and p is the pitch of sheet/purlin fasteners.

For connections to rafters,

$$c_{32} = \frac{2s_{sc}}{n_{sc}} \quad (4 \text{ sides fastened}) \quad (13)$$

$$c_{32} = \frac{2}{n_p} \left(s_{pr} + \frac{s_p}{\beta_2} \right) \quad (2 \text{ sides only fastened}) \quad (14)$$

Where s_{sc} is the slip per sheet/shear connector fastener per unit load, n_{sc} is the number of sheet/shear connector fasteners per end rafter, n_p is the number of purlins and s_{pr} is the deflection of top of purlin at purlin/rafter connection per unit load.

For seam fasteners,

$$c_{33} = \frac{2s_s s_p (n_{sh} - 1)}{2n_s s_p + \beta_1 n_p s_s} \quad (15)$$

Where n_{sh} is the number of sheet widths per shear panel.

5.2.4 Flexibility due to axial deformation of the frame (c_4)

The axial force in the frame is assumed to be triangular varying linearly from a maximum value at one end to zero at the other end. Using a strain energy approach:

$$c_4 = \frac{2a^3}{3EAb^2} \quad (16)$$

Where A is the cross-sectional area of a longitudinal edge member.

5.2.5 Design equation for stiffness

The equation for stiffness can be derived as:

$$\begin{aligned}
c_s &= \frac{1}{k_s} = c_1 + c_2 + c_{31} + c_{32} + c_{33} + c_4 \\
&= \frac{2a(1+\nu)[1+(2h/d)]}{Et b} + \frac{ad^{2.5}\alpha_1\alpha_2 K}{Et^{2.5}b^2} + \frac{2as_p p}{b^2} + \frac{2s_{sc}}{n_{sc}} + \frac{2s_s s_p (n_{sh}-1)}{2n_s s_p + \beta_1 n_p s_s} + \frac{2a^3}{3EA b^2}
\end{aligned} \quad (17)$$

6. Comparison of finite element results with EUR formulas and tests

The determination of strength and stiffness of test shear diaphragms is crucial to stressed skin theory. The stiffness G of test diaphragms (N/mm) is defined as the reciprocal of the slope of the linear part of the above load-displacement curve. The shear strength P_u is defined as the maximum load sustained. The shear stiffness G can be calculated from the graph of load against displacement as follows:

$$G = \frac{0.6P_u}{\Delta} \quad (18)$$

where Δ is mean displacement at a load of $0.6P_u$ and P_u is the shear strength.

The ultimate loads and shear stiffness predicted by the FEA are compared with the experimental results of the stressed skin diaphragms and predictions from the formulas of EUR, as are summarized in Table 3. For comparison purpose, the computing errors of experimental and FEA results are shown in the Table 4. It is shown that results obtained from the FEA are in good agreement the experimental results. Generally, the FEA ultimate shear loads are slightly conservative for the test series, except for the specimen SJ1-1 of Series T1. The FEA shear stiffness are slightly smaller than the experimental

Table 3 Comparisons of Strength and stiffness calculated by FEA, TEST and EUR

Test Series number	Specimens Number	Shear Strengths (KN)			Shear Stiffness (N/mm)		
		Test	Finite Element	EUR formula	Test	Finite Element	EUR formula
T1	SJ1-1	11.58	12.88	10.63	1012.7	1112.215	1002.6
	SJ1-2	13.2			934.4		
T2	SJ2	17.8	16.41	14.18	1095.05	1133.521	1176
T3	SJ3-1	13.71	11.09	8.38	568.57	512.61	487
	SJ3-2	12.71			572.57		
T4	SJ4	14.34	13.03	8.38	640.1	698.47	722

Table 4 Computing errors between the results of FEA and TEST

Test Series number	Shear Strengths			Shear Stiffness		
	Test (KN)	Finite Element (KN)	Errors (%)	Test (N/mm)	Finite Element (N/mm)	Errors (%)
T1	12.39	12.88	-3.95	973.5	1112.22	-14.3
T2	17.8	16.41	7.8	1095.05	1133.52	-3.52
T3	12.21	11.09	9.17	570.6	512.61	10.16
T4	14.34	13.03	9.14	640.	698.47	-9.12

Note: error(%) = (experimental value-FEA value)/ experimental value×100%

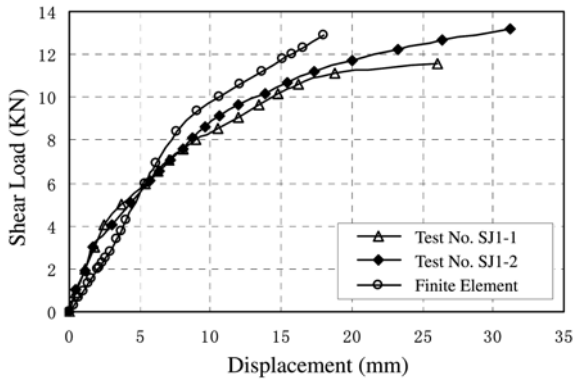


Fig. 17 Comparisons of the load-displacement curves; Test Series 1

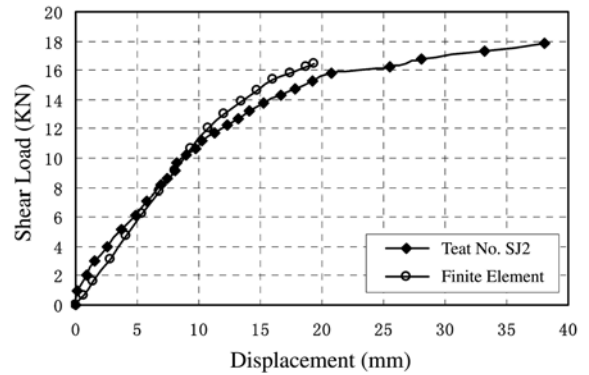


Fig. 18 Comparisons of the load-displacement curves; Test Series 2

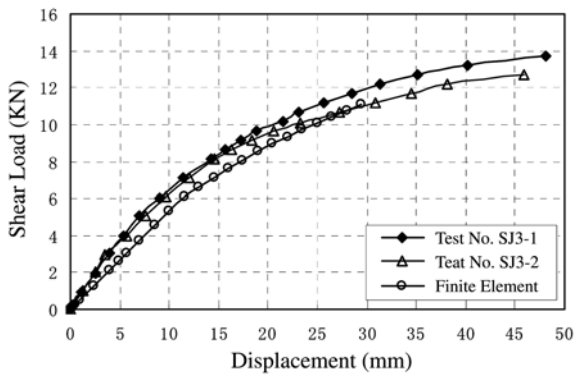


Fig. 19 Comparisons of the load-displacement curves; Test Series 3

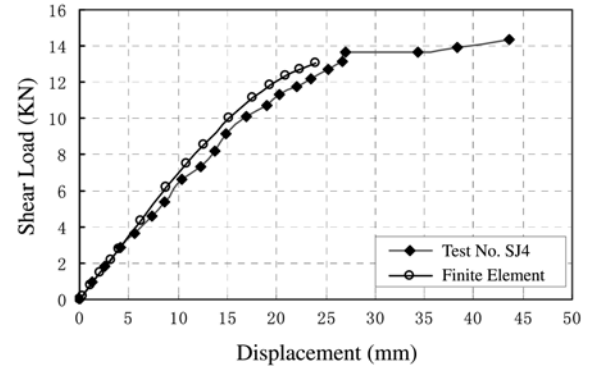


Fig. 20 Comparisons of the load-displacement curves; Test Series 4

results, except for the Series T3 with the error of 10.6%. The strength values calculated by EUR formulas are smaller than the corresponding experimental and finite element values. Calculated strength occurs on the safe side for the reason that in the EUR design formulas the values of the fastener strength are the design strength considering the safe factor of fastener shear capacity. However, the experimental and finite element values are the results that caused by the ultimate shear loads of fasteners.

Figs. 17, 18, 19 and 20 compare the shear load versus displacement curve predicted by the FEA with the corresponding experimental curve for series T1, T2, T3 and T4. It is shown that the FEA curve follows closely the experimental curve in the linear range. Such an agreement in terms of displacement between the numerical and tests results provides confidence in the model applied in this investigation. A small discrepancy between the two curves is observed into the nonlinear load-displacement range.

Fig. 21(a) shows the photograph of specimen SJ3-1 after the ultimate load has reached. Fig. 21(b) shows the deformed shape of the specimen predicted by the FEA right after the ultimate load. The resemblance of the Fig. 21(a) and (b) demonstrates the reliability of the FEA predictions.

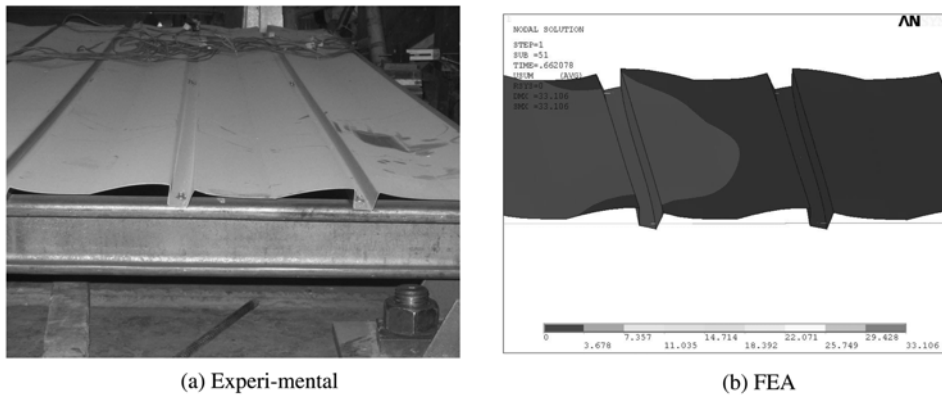


Fig. 21 Comparison of experimental and FEA deformed shapes for Specimen SJ3-1

7. Conclusions

A detailed finite element model that simulates the diaphragm has been developed in this paper. The skin of the sheeting in this model was simulated using shell elements while the fastener was simulated using a nonlinear spring system. The force-displacement characteristics for the spring elements were determined based on the result of joint tests program. The finite element model was then evaluated by comparing its results to those obtained from the full-scale tests.

Having verified the developed finite element model, the shear behavior of the diaphragm made was studied and the following conclusions were drawn:

- (1) Test frames, supporting the profiles sheeting, had negligible stiffness.
- (2) Results of full-scale test indicate that the shear behavior was affected by the profiled sheeting configuration, purlin spacing and arrangements of fasteners. Two types of panel configuration were tested, however, the shear strength and stiffness were different; shear strength of panel was increased by a reduction of spacing and stiffness of panel was not particularly sensitive to changes in span.
- (3) The results of the simulation show that the above proposed finite element model, using the non-linear finite element program ANSYS, provides a simulation which agrees well with the tests. Therefore, the model can be used for the prediction of the shear behavior of the stressed skin diaphragm and can further be applied to relevant parametric studies.

References

- AISI. (1967), "Design of light gauge steel diaphragms", New York. N.Y.
- ANSYS Corporation (2004), Structural Analysis Guide.
- Bryan, E. R. (1972), "The stressed skin design of steel buildings", Grosby Lockwood Staples, London.
- Bryan, E. R. and El-Dakhakhi, W. M. (1968), "Shear flexibility and strength of corrugated decks", *J. Struct. Div.*, ASCE, **94**(ST11), 2549-2579.
- Davies, J. M. (1976), "Calculation of steel diaphragm behavior", *J. Struct. Div.*, ASCE, **102** (ST11), 1411-1430.
- Davies, J. M. (1977), "Simplified diaphragm analysis", *J. Struct. Div.*, ASCE, **103**(ST11), 2093-2109.
- Davies, J. M. and Bryan, E. R. (1982), *Manual of Stressed Skin Diaphragm Design*, Granada, London.
- Davies, J. M. and Fisher, J. (1979), "The diaphragm action of composite slabs", *Proc. Institution of Civil Engineers*,

- London, England, **67**(2), 891-906.
- Easley, J. T. (1975), "Buckling formulas for corrugated metal shear diaphragms", *J. Struct. Div.*, ASCE, **101**(ST7), 1403-1417.
- Easley, J. T. (1977), "Strength and stiffness of corrugated metal shear diaphragms", *J. Struct. Div.*, ASCE, **103**(ST1), 169-180.
- Easterling, W. S. and Porter, M. L. (1994), "Steel-deck-reinforced concrete diaphragms I", *J. Struct. Eng.*, ASCE, **120**(2), 560-576.
- ECCS (1995), European Recommendations for the Application of Metal Sheeting acting as a Diaphragm. Pub. **88**, European Convention for Constructional Steelwork, Brussels.
- El-Dakhkhni, W. M. (1976), "Shear of light gauge partitions in the tall buildings", *J. Struct. Div.*, ASCE, **102**(ST7), 1431-1445.
- Fazio, P. F., Kinh, H. A. and Chockalingam, S. (1978), "Strength of cold-formed steel shear diaphragms", *Canadian J. Civ. Eng.*, 5-17.
- Luttrell, L. D. (1971), "Shear diaphragms with lightweight concrete fill", *Proceedings of the 1st Specialty Conference on Cold-Formed Steel Structures*, University of Missouri-Rolla, 111-117.
- Nilson, A. H. (1960), "Shear diaphragms of light gage steel", *J. Struct. Div.*, ASCE, **86**(ST11), 11-139.
- Nilson, A. H. and Ammar, A. R. (1974), "Finite element analysis of metal deck shear diaphragms", *J. Struct. Div.*, ASCE, **100**(ST4), 711-725.

CE